European Journal of Radiology 121 (2019) 108733

Contents lists available at ScienceDirect

European Journal of Radiology

journal homepage: www.elsevier.com/locate/ejrad

Review

CT artifacts from port systems: Virtual monoenergetic reconstructions from spectral-detector CT reduce artifacts and improve depiction of surrounding tissue

Kai Roman Laukamp[a,b,c,*], David Zopfs[a], Anton Wagner[a], Simon Lennartz[a], Lenhard Pennig[a], Jan Borggrefe[a], Nikhil Ramaiya[b,c], Nils Große Hokamp[a,b,c]

[a] Institute for Diagnostic and Interventional Radiology, Faculty of Medicine and University Hospital Cologne, University of Cologne, Kerpener Straße 62, 50937, Cologne, Germany
[b] Department of Radiology, University Hospitals Cleveland Medical Center, 11000 Euclid Ave, 44106 Cleveland, OH, USA
[c] Department of Radiology, Case Western Reserve University, 10900 Euclid Ave, 44106, Cleveland, OH, USA

ARTICLE INFO

Keywords:
X-ray computed tomography
Artifacts
Neoplasm staging
Port system

ABSTRACT

Purpose: CT artifacts from port-systems are a common problem in staging- and restaging-examinations and reduce image quality and diagnostic assessment. The purpose of this study was to investigate the reduction of these artifacts using virtual monoenergetic images (VMI) from dual-energy spectral-detector CT (SDCT) in comparison to conventional CT-images (CI).

Method: 50 SDCT-datasets of patients with artifacts from port-chamber and port-catheters were included in this IRB-approved, retrospective study. CI and VMI (range, 40–200 keV, 10 keV increment) were reconstructed from the same acquisition. The quantitative image analysis was performed ROI-based assessing mean and standard deviation of attenuation (HU) in most pronounced hypo- and hyperdense artifacts surrounding to the port-chamber and the distal end of the port-catheter in the superior vena cava. Subjectively, artifact reduction and diagnostic assessment of surrounding soft tissue were rated on 5-point Likert-scales.

Results: In comparison to CI, VMI of higher keV-values showed strong reduction of hypo- and hyperattenuating artifacts around the port-chamber and port-catheter (CI/VMI_{200keV}: hypodense −104.7 ± 124.7HU/10.8 ± 58.1HU and −101.6 ± 101.5HU/−36.7 ± 32.9HU; hyperdense 240.8 ± 151.6HU/79.6 ± 81.3HU and 108.6 ± 129.3HU/25.9 ± 31.9HU; all $p < 0.001$). Image noise could also be reduced significantly. The subjective analysis showed significantly reduced artifacts around the port-chamber and port-catheter (CI/VMI_{200keV}: hypodense 3(1–4)/5(4–5) and 3(2–4)/5(4–5); hyperdense 3(1–4)/5(4–5) and 3(2–3)/5(3–5); all $p < 0.001$) and improved diagnostic assessment of pectoral/subclavian soft tissue for VMI of ≥100keV. Ratings for diagnostic assessment were best between 140 − 200 keV. Overall interrater agreement was high (ICC = 0.79).

Conclusions: Higher keV VMI enabled a significant reduction of artifacts from port-systems around the chamber and the catheter leading to improved assessment of surrounding soft tissue.

1. Introduction

Port systems cause hypo- and hyperdense artifacts in CT imaging as they partly consist of metal alloys. In addition highly attenuating contrast media can remain within the port system after contrast media injection [1–3]. Three types of artifacts can be differentiated, i.e. beam-hardening, photon starvation, and scatter artifacts [4–8]. Combined, these artifacts cause interferences that negatively impact image quality and diagnostic assessment of surrounding structures, i.e. lymph nodes, muscles, vessels, fat and bone. This is of special relevance in oncologic staging and restaging examinations, as soft tissue and lymph node metastases may be obscured [1,9,10]. Further, evaluation of non-occlusive thrombi associated to the distal tip of the port catheter may be hampered by artifacts from the catheter itself [1,9].

Port placement is common in cancer patients and facilitates application of drugs and administration of contrast media which is required

Abbreviations: CI, conventional CT imaging/images; SDCT, spectral-detector CT; VMI, virtual monoenergetic images; HU, hounsfield unit

* Corresponding author at: Institute for Diagnostic and Interventional Radiology, Faculty of Medicine and University Hospital Cologne, University of Cologne, Kerpener Straße 62, 50937, Cologne, Germany.
E-mail address: kai.laukamp@uk-koeln.de (K.R. Laukamp).

https://doi.org/10.1016/j.ejrad.2019.108733
Received 30 April 2019; Received in revised form 19 October 2019; Accepted 27 October 2019

for most multidetector CT injection protocols to achieve adequate image quality [2,3,9]. To avoid residual contrast media within the port system, a saline flush is routinely applied. Still, contrast media residues may remain in the port chamber and catheter potentially worsening artifacts [1–311].

Dual-energy CT (DECT) allows for the reconstruction of virtual monoenergetic images (VMI) that effectively reduce artifacts caused by highly attenuating metal material and contrast media [1,12]. VMI correspond to CT images that would result from acquisitions with true monoenergetic x-rays which at higher keV-levels are more resistant to beam hardening [13–15]. The spectral-detector CT (SDCT) has a single x-ray source and detects low- and high-energetic photons separately on the detector level. Similar to other DECT systems VMI can be extrapolated as linear blends from the two registered energy levels [13]. SDCT registers high- and low-photon energies in both temporal and spatial coherence allowing computation of VMI in projection opposed to the image domain which is not possible for all other DECT solutions [13,16]. High-keV VMI from the different DECT systems have shown their dedicated value for the reduction of artifacts for different types of metal implants and devices, e.g. total hip replacements, orthopedic hardware of the spine, dental implants and coils as well as clips [7,8,12,17–21]; however, usefulness in port systems has not been investigated yet.

This study investigates if artifacts caused by the port chamber and the distal tip of the port catheter can be reduced using virtual monoenergetic images from SDCT. Also, we evaluated if and to what extent diagnostic assessment of the surrounding soft tissue in staging and restaging examinations can profit from these reconstructions. To evaluate the influence of contrast media causing artifacts next to the port system itself we included an additional phantom acquisition.

2. Material and methods

2.1. Patient selection

This retrospective study was approved by the institutional review board. It was conducted in accordance with the ethical regulations of the 1964 Helsinki declaration and its later amendments. Due to the retrospective design informed consent was waived. The following criteria for inclusion were applied: (i) age: ≥18 years, (ii) combined thoracoabdominal staging and restaging examinations in portal venous phase between November 2017 and March 2018, (iii) patients with a port system that was used for administration of contrast media, and (iv) artifacts surrounding the port system with impairment of diagnostic assessment of surrounding soft tissue. The criteria were applied by a radiologist with three years of experience in oncologic imaging. Fifty consecutive patients were included in the final analysis. All scans were conducted for clinical reasons only and no scan was acquired explicitly for the purpose of this study.

2.2. Imaging protocol

A clinical SDCT scanner (IQon, Philips Healthcare) was used for all examinations. Patients were placed in a head-first supine position. Iodinated contrast media (Accupaque 350 mg/ml, GE Healthcare) was administered by the port system, followed by a 30 ml saline flush. Flow rates were between 3–4 ml/s. If a patient's port system would not support flow rates this high, a peripheral venous catheter was used instead; however, these patients were not included in this study. Scans were initialized with a 50 s delay after exceeding a threshold value of 150 Hounsfield units (HU) in the descending aorta. Following scan parameters were used: matrix 512 × 512, collimation 64 × 0.625 mm, rotation time 0.33 s, pitch 0.671, tube voltage 120 kVp. All examinations were conducted with automatic tube current modulation (DoseRight 3D-DOM, Philips Healthcare). In addition, a plain port (PowerPort Slim Titanium device with 6 Fr. Attachable Polyurethane Catheter, Bard Access Systems) placed in a non-anthropomorphic water phantom was imaged using the above specified protocol. The water phantom was scanned two times, once with contrast media administered to the port system and once after a saline flush for elimination any contrast media residues.

Conventional CT images (CI) and VMI (range: 40–200 keV, increment of 10 keV) were automatically created with every scan using the standard spectral reconstruction algorithm (Spectral B, Philips Healthcare). Slice thickness and section increment for reconstruction in axial plane were set to 2 mm and 1 mm, respectively. The following analyses were conducted using the proprietary image viewer (Intellispace Portal, Philips Healthcare) allowing simultaneous access and image analysis for CI as well as VMI.

2.3. Objective analysis

A radiologist with three years of experience in oncologic imaging conducted the image assessment in axial image reconstructions (window settings: soft tissue, window level: 60, window width: 360). Circular regions of interest (ROI) with a defined size of 100 mm^2 were placed on CI and then copied to VMI. To avoid unrepresentative tissue, ROI size could possibly be reduced depending on the individual case. This was more often necessary for artifacts surrounding the port catheter as artifacts here were less pronounced compared to the port chamber. ROI were placed in most pronounced hypo- and hyperdense artifacts surrounding the port chamber and the distal tip of the port catheter in the vena cava superior, as well as in corresponding artifact-free reference tissue (e.g. when the hypodense artifact impaired muscle the reference tissue was artifact-free muscle). Mean and standard deviation of attenuation were recorded.

Attenuation changes along different keV-values in VMI (e.g. at higher keV-values, attenuation of muscle as well as arteries decreases and attenuation of fat increases [13]). To avoid interference of this effect with artifact reduction-related attenuation changes, we calculated the corrected attenuation as the difference between HU-values in soft tissue (hypo- and hyperdense artifact) with visual presence of artifacts and corresponding reference tissue without artifacts, as previously applied [8]. Analogously, corrected image noise was calculated to account for a generally lower image noise in high-keV VMI reconstructions, as previously suggested [8,13,17].

2.4. Subjective analysis

5-point Likert-scales were used by the subjective readers (two radiologists with two and three years of experience in oncologic imaging) to evaluate the extent of hypo- and hyperdense artifacts surrounding the port chamber and the port catheter. Additionally, they evaluated diagnostic assessment (being possibly impaired by artifacts)

Table 1
Visual analysis.

Extent of hypo- and hyperdense artifacts from the port chamber and catheter	(5) artifacts are absent/almost absent; (4) minor artifacts; (3) moderate artifacts, (2) pronounced artifacts; (1) massive artifacts
Diagnostic assessment of the pectoral/axillary soft tissue surrounding the port (muscle, fat, lymph nodes)	5) full diagnostic quality as there are no artifacts/almost no artifacts; (4) marginally affected diagnostic quality by minor streaks; (3) hampered diagnostic quality by moderate artifacts; (2) restricted diagnostic quality by strong artifacts; (1) insufficient diagnostic quality

of soft tissue surrounding the port chamber. Further, introduction of new artifacts was rated by the readers. Detailed rating criteria are reported in Table 1. The readers were provided with a full set of images for each patient; however, which series corresponded to which reconstruction/energy was not explicitly known to the readers (although true blinding appeared not feasible due to visual different appearances of the different reconstructions). In addition, readers were blinded to the results of the objective analysis.

CI as well as VMI at 70, 100, 140 and 200 keV were assessed in the qualitative assessment. Larger increments compared to the objective analysis were chosen to detect relevant changes in image quality and not to obscure differences by evaluation of too similar images, as it has been suggested before [1,12,22]. Image parameters for visual assessment: slice thickness of 2 mm, axial plane and soft tissue window settings (center/width, 60/360). As artifacts show a strong dependence on appropriate window settings, the readers were explicitly free to adjust them.

2.5. Statistical analysis

Statistical analyses were conducted using JMP Software (JMP v12, SAS Institute). Results from the quantitative analysis are written as mean ± standard deviation and qualitative results as median Likert scores and 10/90-percentile. The Shapiro-Wilk test was used to test for normal distribution. For further analyses the Wilcoxon-test with Steel adjustment for multiple comparisons was applied. Statistical significance was defined as $p < 0.05$. The intraclass correlation coefficient was used to assess interreader agreement in the visual analysis.

3. Results

3.1. Patient data

50 patients were included in the final analysis. These patients were affected by hypo- and hyperattenuating artifacts along the port system that impaired diagnostic assessment. The average age was 59.2 ± 11.2 years (range: 22–78 years). Thirty-one patients were female and 19 were male. All patients were in an oncologic setting and had a history of the following neoplasms: breast cancer n = 13, lung cancer n = 8; gynecological cancer (ovary, cervix, uterus) n = 8, malignant melanoma n = 6; pancreatic cancer n = 3, gastric cancer n = 3, esophageal cancer n = 3, urothelial cancer n = 2, lymphoma n = 2, and other cancer types n = 2.

3.2. Objective assessment

3.2.1. Corrected attenuation

The corrected attenuation increased significantly within the hypodense artifacts around the port chamber at higher VMI keV-values from 100 − 200 keV (Figs. 1A, 3 & 4 Table 2). Further, VMI of ≥110 keV significantly decreased corrected attenuation in hyperdense artifacts around the port chamber (Figs. 1A, 3 & 4 Table 2). In addition, the corrected attenuation values reached 0 HU between 140 and 150 keV for hypodense artifacts and even turned positive within hypodense artifacts at higher keV-values, e.g. VMI at 200 keV, 10.8 ± 58.1 HU (Figs. 1A & 4 Table 2). In line with the port chamber artifacts, the port catheter artifacts at higher-keV VMI displayed a significant increase and decrease of the corrected attenuation within the hypodense (≥130 keV) and hyperdense (≥110 keV) artifacts, respectively (Figs. 1B, 4 & 5 Table 2).

3.2.2. Corrected image noise

The corrected image noise was found significantly lower at higher keV-levels for hypodense artifacts of the port chamber as well as for hypo- and hyperdense artifacts surrounding the port catheter (Fig. 2, Table 2).

3.2.3. Subgroup analysis

Nine patients showed relevant residues of contrast media in the port chamber. Visually, these patients suffered from stronger artifacts around the port chamber. Accordingly, HU-values in these patients were lower in hypodense (contrast media residues/no contrast media residues: - 243.0 ± 129.4/- 77.0 ± 104.9 HU, $p = 0.0025$) and higher in hyperdense artifacts as compared to patients without residues (contrast media residues/no contrast media residues: 352.3 ± 166.7/ 201.5 ± 127.9 HU, $p = 0.043$), respectively. The HU-values of artifacts around the port catheter did not differ significantly between these groups (hypodense, contrast media residues/no contrast media residues: - 64.1 ± 80.5/- 108.5 ± 104.3 HU, $p = 0.25$; hyperdense, contrast media residues/no contrast media residues: 131.9 ± 46.9/ 104.1 ± 140.0 HU, $p = 0.073$).

3.3. Phantom examination

In the phantom acquisition, hypodense artifacts were pronounced compared to hyperdense artifacts. These artifacts were strongest around the port chamber and the distal tip of the port catheter (Fig. 4). In both phantom acquisitions these artifacts were present, in Fig. 4A where a saline flush had been applied to eliminate any contrast media residues and in Fig. 4B where no saline flush had been administered after contrast media administration (Fig. 4B). The artifacts were stronger in presence of contrast media residues (Fig. 4B). VMI ≥ 100 keV showed an effective reduction of these artifacts. Initial hypodense artifacts around the port chamber even turned hyperdense in VMI ≥ 140 keV.

3.4. Visual assessment

The subjective findings were in line with the objective results. Both hypo- and hyperdense artifacts were significantly reduced around the port chamber and the port catheter using higher VMI keV-values (≥100 keV) with best results in 200 keV images (Figs. 3–5, Table 3). The diagnostic assessment of the pectoral/axillary soft tissue surrounding the port (muscle, lymph nodes, vessels and fat) and diagnostic confidence was significantly improved by VMI of ≥100 keV, reaching a plateau between 140 − 200 keV (Fig. 3, Table 3). The readers did not notice an introduction of new artifacts by VMI that impaired image quality or diagnostic assessment (Fig. 4). Overall interrater agreement was good (intraclass correlation coefficient = 0.78). Table 2 provides detailed results on interreader agreement.

4. Discussion

Oncologic CT imaging is often hampered by artifacts from ***port systems*** occurring along the chamber and the catheter. This study investigated reduction of these artifacts comparing VMI to conventional CT images. VMI showed an effective and significant reduction of hypo- and hyperdense artifacts that impaired pectoral and axillary soft tissue surrounding the port chamber as well as vessel lumen along the catheter. The improved image quality also led to a better diagnostic assessment and higher diagnostic confidence for evaluation of soft tissue surrounding the port chamber. In clinical practice oncologic staging examinations are a common task and detection of lymph node and soft tissue metastases is of pivotal importance for therapy decisions and patient prognosis. Aiming for excellent image quality, e.g. by reducing artifacts from port chambers, is therefore an important task in imaging of these patients. Breast cancer patients might profit most as metastases of the chest wall and axilla are more common due to the primary location of the cancer and its metastatic pathways [23]. Further, oncologic patients are more often affected by vessel pathologies, by reduction of artifacts the evaluation of axillary and subclavian vessel pathologies, such as venous thrombosis or arterial stenosis, might be facilitated [5,6]. Detection and characterization of catheter associated non-occlusive thrombi at the distal tip of the port catheter should also

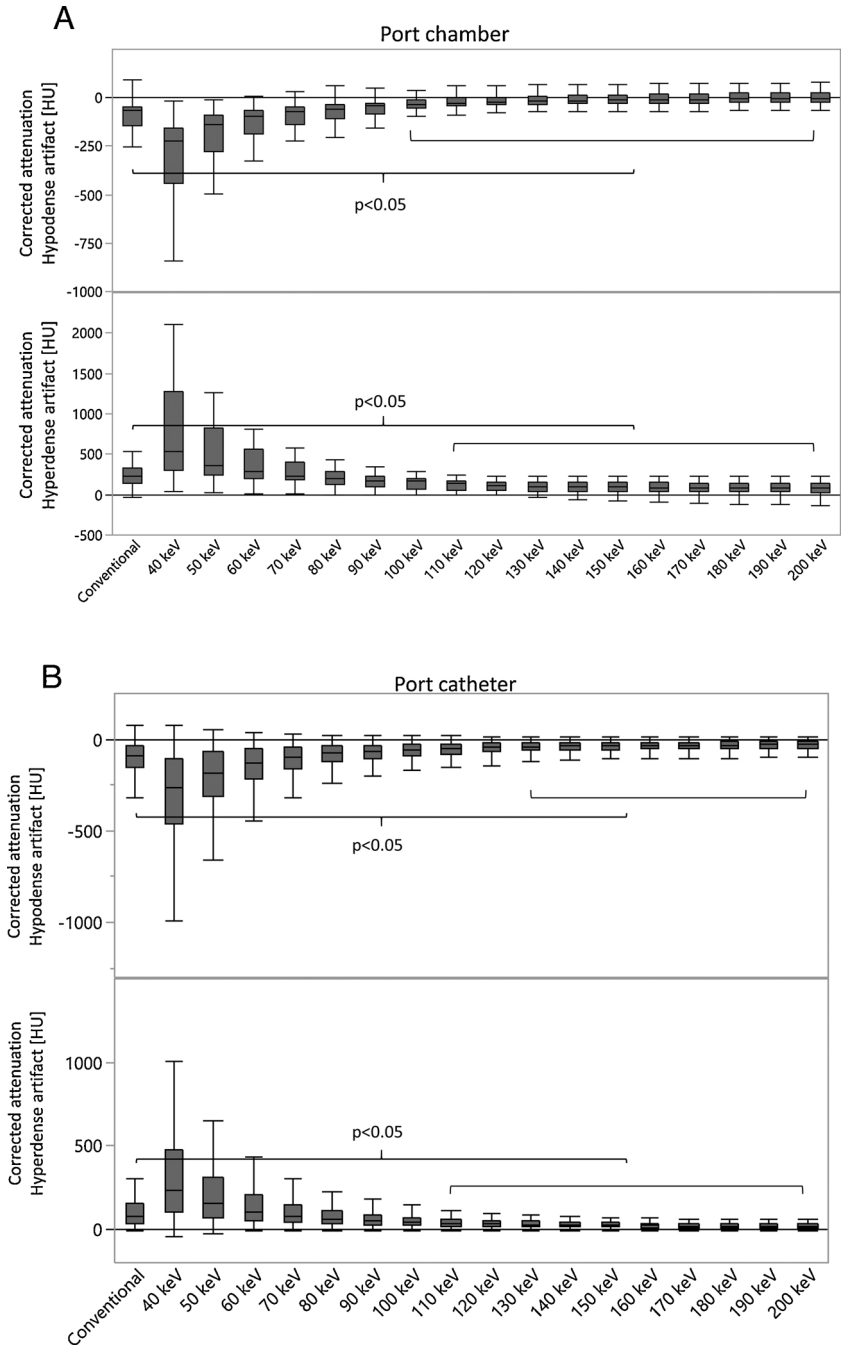

Fig. 1. Box-plot diagram displaying corrected attenuation values in hypo- and hyperdense artifacts A) around the port chamber and B) around the port catheter in conventional CT images (CI) and virtual monoenergetic images (VMI, 40–200 keV). A) Port chamber: VMI of 100/110 keV or higher significantly reduce hypo-/hyperdense artifacts. B) Port catheter: VMI of 130/110 keV or higher significantly reduce hypo-/hyperdense artifacts.

be facilitated by an effective artifact reduction as presented in our study [5,6,9]. Port systems can suffer from several mechanical complications, such as disconnection of the catheter, dislocation and leakage [24,25]. Reducing port artifacts should facilitate detection of these complications.

Further, dual-energy acquisitions are always enabled in spectral-detector CT due to the detector-based separation of photons (which is not the case for tube-based dual-energy CT systems), thereby VMI can always be applied and adjusted to the correct keV-level whenever port artifacts occur, which should benefit workflow in clinical practice [13].

Our results are supported by current literature investigating artifact reduction using VMI. Although reduction of artifacts due to port systems has not been investigated so far, high-keV VMI showed effective metal artifact reduction and improved diagnostic assessment in various locations as well as indications [7,8,12,17–21]. Despite different characteristics regarding image noise, the utility of high keV VMI images has been demonstrated for all major dual-energy solutions (i.e. dual-source, rapid kilovolt-switching and dual-layer spectral-detector), [26,27].

Port systems consist of metal and may contain residual contrast media at the time of the scan, especially when technical difficulties occur that hamper or prevent administering a saline flush [1,3,6]. A subgroup analysis in our study revealed that relevant residues of contrast media in the port chamber enhanced artifact severity and were thereby partly responsible for port artifacts next to metal material. This could also be seen in the phantom acquisition where artifacts around

Table 2
Objective assessment of artifact reduction and surrounding tissue.

	Corrected attenuation/HU-values				Corrected image noise/standard deviation			
	Port body		Port catheter		Port body		Port catheter	
	Hypodense artifact	Hyperdense artifact	Hypodense artifact	Hyperdense artifact	Hypodense artifact	Hyperdense artifact	Hypodense artifact	Hyperdense artifact
CI	−104.7 ± 124.7	240.8 ± 151.6	−101.6 ± 101.5	108.6 ± 129.3	34.2 ± 40.4	29.3 ± 49.5	23.7 ± 64.9	81.7 ± 120.6
VMI								
70 keV	−108.0 ± 109.9	260.9 ± 152.6	−112.5 ± 96.1	106.9 ± 125.8	33.3 ± 42.1	29.8 ± 46.9	29.9 ± 22.8	72.0 ± 110.9
80 keV	−72.2 ± 73.7	206.2 ± 110.3	−89.7 ± 74.9	82.5 ± 96.1	24.0 ± 31.0	24.0 ± 38.5	23.3 ± 17.7	54.5 ± 84.8
90 keV	−48.7 ± 54.5	170.5 ± 87.9	−74.7 ± 61.6	66.6 ± 77.1	18.1 ± 24.2	20.3 ± 33.7	19.2 ± 14.6	**43.2 ± 68.1**
100 keV	**-32.8 ± 46.3**	146.2 ± 77.5	−64.6 ± 52.9	55.7 ± 64.4	**14.3 ± 20.0**	17.8 ± 30.7	16.4 ± 12.6	**35.6 ± 57.9**
110 keV	**-21.6 ± 44.4**	**129.1 ± 73.6**	−57.3 ± 47.2	**48.0 ± 55.6**	**11.8 ± 17.2**	16.1 ± 28.9	14.6 ± 11.3	**30.2 ± 49.4**
120 keV	**-13.5 ± 45.4**	**116.7 ± 72.9**	−52.3 ± 43.1	**42.4 ± 49.5**	**10.2 ± 15.5**	14.9 ± 27.7	**13.2 ± 10.4**	**26.3 ± 44.1**
130 keV	**-7.4 ± 47.3**	**107.4 ± 73.6**	**-48.3 ± 40.3**	**38.4 ± 45.0**	**9.1 ± 14.3**	14.1 ± 27.0	**12.2 ± 9.8**	**23.5 ± 40.2**
140 keV	**-2.8 ± 49.4**	**100.3 ± 74.8**	**-45.4 ± 38.2**	**35.2 ± 41.7**	**8.2 ± 13.4**	13.4 ± 26.4	**11.4 ± 9.4**	**21.4 ± 37.5**
160 keV	**-3.7 ± 53.4**	**90.5 ± 77.4**	**-41.2 ± 35.5**	**30.8 ± 37.2**	**7.3 ± 12.4**	12.6 ± 25.7	**10.3 ± 8.9**	**18.4 ± 33.7**
200 keV	**10.8 ± 58.1**	**79.6 ± 81.3**	**-36.7 ± 32.9**	**25.9 ± 32.7**	**6.5 ± 11.6**	11.8 ± 25.0	**9.2 ± 8.5**	**15.2 ± 29.9**
p-values								
CI vs. VMI 80 keV	$p > 0.05$	$p > 0.05$	$p > 0.05$	$p > 0.05$	$p > 0.05$	$p > 0.05$	$p > 0.05$	$p > 0.05$
CI vs. VMI 90 keV	$p > 0.05$	$p > 0.05$	$p > 0.05$	$p > 0.05$	$p < 0.05$	$p > 0.05$	$p > 0.05$	$p < 0.05$
CI vs. VMI 100 keV	$p = 0.004$	$p > 0.05$	$p > 0.05$	$p > 0.05$	$p = 0.007$	$p > 0.05$	$p > 0.05$	$p = 0.005$
CI vs. VMI 110 keV	$p < 0.001$	$p = 0.019$	$p > 0.05$	$p = 0.009$	$p < 0.001$	$p > 0.05$	$p > 0.05$	$p < 0.001$
CI vs. VMI 120 keV	$p < 0.001$	$p = 0.019$	$p > 0.05$	$p = 0.002$	$p < 0.001$	$p > 0.05$	$p = 0.03$	$p < 0.002$
CI vs. VMI 130 keV	$p < 0.001$	$p = 0.009$	$p = 0.032$	$p < 0.001$	$p < 0.001$	$p > 0.05$	$p = 0.015$	$p < 0.003$
CI vs. VMI 140 keV	$p < 0.001$	$p < 0.003$	$p = 0.012$	$p < 0.001$	$p < 0.001$	$p > 0.05$	$p = 0.015$	$p < 0.001$
CI vs. VMI 160 keV	$p < 0.001$	$p < 0.001$	$p = 0.004$	$p < 0.001$	$p < 0.001$	$p > 0.05$	$p = 0.007$	$p < 0.001$
CI vs. VMI 200 keV	$p < 0.001$	$p < 0.001$	$p = 0.001$	$p < 0.001$	$p < 0.001$	$p > 0.05$	$p = 0.003$	$p < 0.001$

CI - conventional imaging, VMI - virtual monoenergetic images, significant changes in HU-values as compared to CI are marked in bold ($p < 0.05$).

the port catheter were pronounced in the port system that did not receive a saline flush after contrast media application (Fig. 4). Applying VMI and subsequent research has not focused on reduction of artifacts caused by high concentration of contrast media, yet. Only one study by Kim et al. is available that investigated this application and has shown first promising results. Physically, VMI appear to be an ideal approach to address contrast media artifacts, as with higher keV-values the distance to k-edge energy of iodine (≈33 keV) increases and attenuation of iodine decreases [28].

High keV-VMI are also known to reduce image contrast which could negatively affect detection of soft tissue metastases and catheter associated thrombi. This should be considered when keV-values ≥140 keV are used [8,13]. This loss of image contrast was of particular relevance when evaluating the port catheter and surrounding vessel lumen; therefore, we recommend that keV-values do not exceed 140 for evaluation of vessel lumen around the catheter tip. For evaluation of the surrounding soft tissue the reduction in image contrast appeared to be less relevant as best diagnostic assessment was observed in 140–200 keV, which we therefore would recommend for clinical routine. Optimal keV-values for artifact reduction differed between patients; further adequate soft tissue and vessel contrast have to be ensured; therefore, we recommend to individually adjust keV-values for optimal image quality and diagnostic assessment.

Earlier studies reported that VMI at higher keV-levels can lead to an overcorrection or even cause new artifacts [8,17]. Both have been described in higher keV images. Overcorrection occurs in location of the initial artifacts in CI and does not exceed the borders of the initial artifacts. Thus, they do not impair diagnostic assessment in addition to CI and have therefore not been rated as new artifacts. New artifacts would be in a different location or overcorrection that exceeds its initial artifact borders [17]. In our study, this overcorrection could only be observed in the objective analysis; here, corrected HU-values turned from negative to positive values for the hypodense artifacts surrounding the port chamber between 140−150 keV; however, this overcorrection was so little (< 11 HU) that the subjective raters did not perceive it in their subjective analysis. In the phantom acquisition a slight overcorrection was also observed (Fig. 4). As the risk of overcorrection and possibly new artifacts is not excludable, CI remain the standard of care supplemented by VMI.

Iterative metal artifact reduction algorithms are primarily designed and approved for larger metal implants, such as total hip replacement [18]. They were also found advantageous in smaller metal material, such as dental implants and coils as well as clips, especially when severe artifacts were present [8,20]. Further, application in coronary CT-angiographies could also raise image quality [29]. Application in port systems might also be effective; however, as shown in our study highly attenuating contrast was partly also responsible for artifacts and it remains at least to some extend unclear how well iterative artifact reduction algorithms work for these kinds of artifacts. In a future study this could be prospectively tested, as these algorithms are mostly dependent on raw image data and therefore not retrospectively available.

The following limitations need to be considered. Different methods can be applied for quantification of artifacts, yet recording HU-values is the most common and frequently used method [18,20]; however, more complex methods have also been used, such as specialized algorithms within the image or projection domain that enable artifact

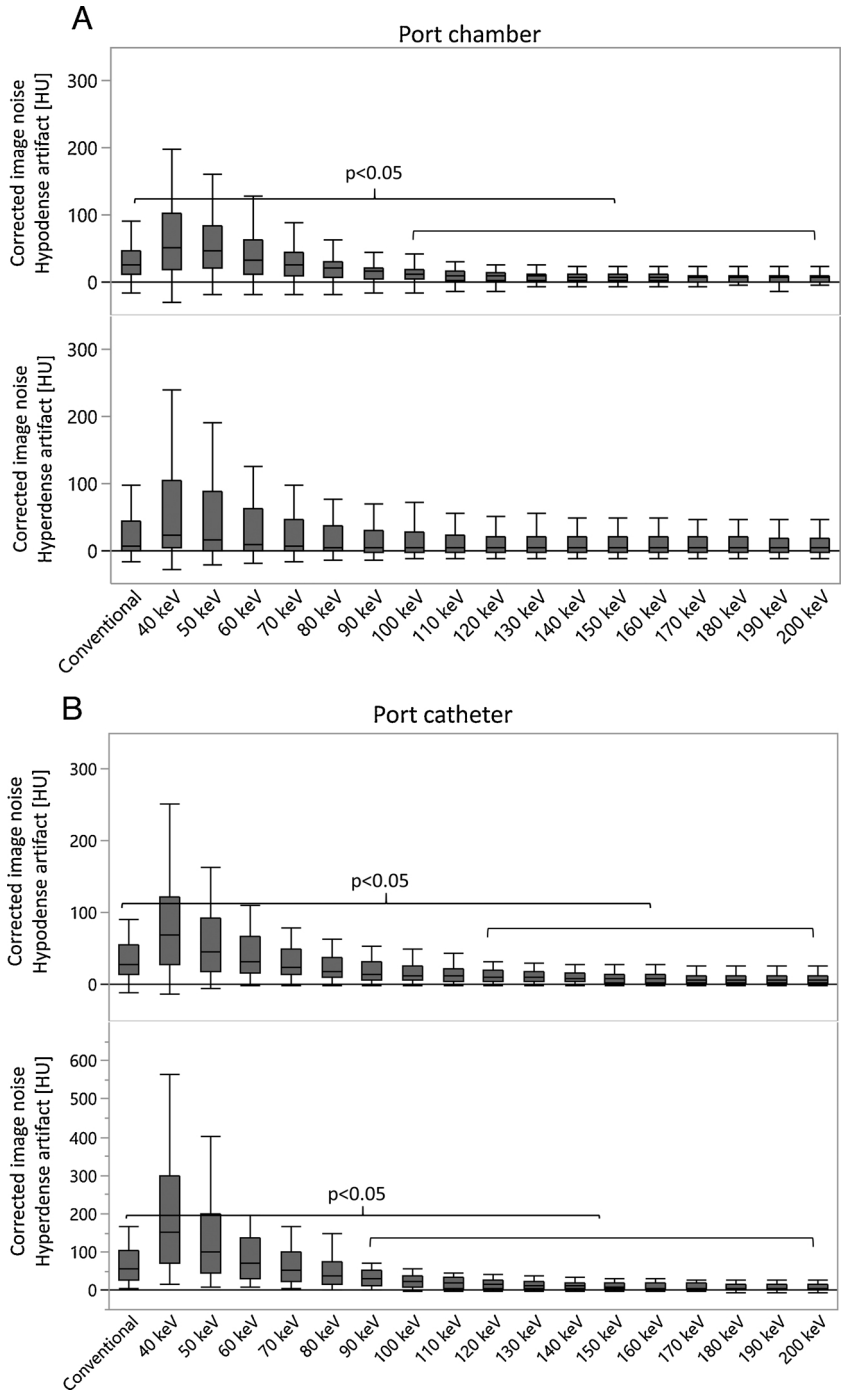

Fig. 2. A) Box-plot diagram displaying corrected image noise in hypo- and hyperdense artifacts A) around the port chamber and B) around the port catheter in conventional CT images (CI) and virtual monoenergetic images (VMI, 40–200 keV). Image noise significantly decreases in hypodense artifacts surrounding the port chamber and in hypo- and hyperdense artifact surrounding the port catheter. Image noise in hyperdense artifacts surrounding the port cannot be reduced significantly by VMI.

quantification [30]. General changes in attenuation and image noise appear with changing VMI keV-values due to their differing physical properties [13]. In order to detect real artifact reduction exclusively and to avoid implying general changes of attenuation and image noise we conducted an intra-individual comparison between artifact impaired tissue and correspondent reference tissue not impaired by artifacts resulting in the corrected image noise and corrected attenuation [8,17]. Due to smaller artifacts around the port catheter, here ROI size needed to be reduced more frequently. As ROI size influences standard deviation this needs to be considered as an additional confounder for image noise. Possible limitations by the objective analyses should be accounted by our detailed subjective analysis by two experienced and independent subjective readers evaluating both artifact reduction and diagnostic assessment. It needs to be considered that we did not aim for a complete blinding as image reconstructions (CI, VMI) were distinguishable by their appearances. Further, next to a qualitative rating of image quality we aimed to encourage readers to appreciate subtle differences between reconstructions; therefore, readers were always presented with a full image set of one patient at a time. High interrater agreement and clear results support the objective findings validate their

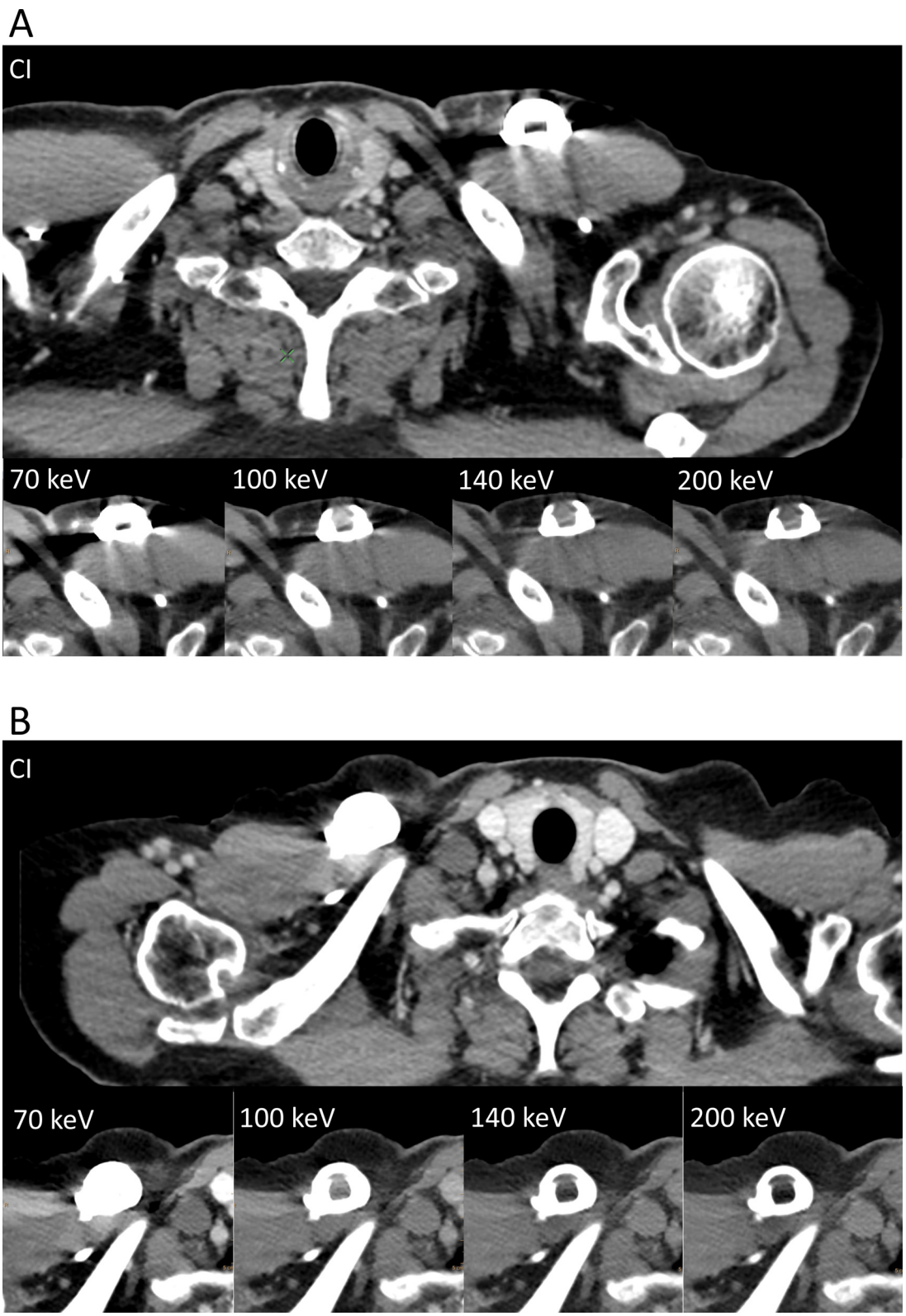

Fig. 3. Images were reconstructed as conventional (CI) and virtual monoenergetic images (VMI, 70 keV, 100 keV, 140 keV and 200 keV) in axial planes (window center/width: 60/360 for all images).
A) Depicted is a 53-year-old patient with esophageal cancer and a port chamber in the left chest wall. The pronounced hypodense and moderate hyperdense artifacts impair the assessment of the surrounding soft tissue. VMI ≥ 100 keV reduce these artifacts and improve diagnostic assessment of adjacent soft tissue. Optimal artifact reduction is achieved by VMI between 140 – 200 keV.
B) Depicted is a 45-year-old patient with breast cancer and a port chamber in the right chest wall. VMI ≥ 140 keV allow for a complete reduction of the moderate hypodense and rather mild hyperdense artifacts.

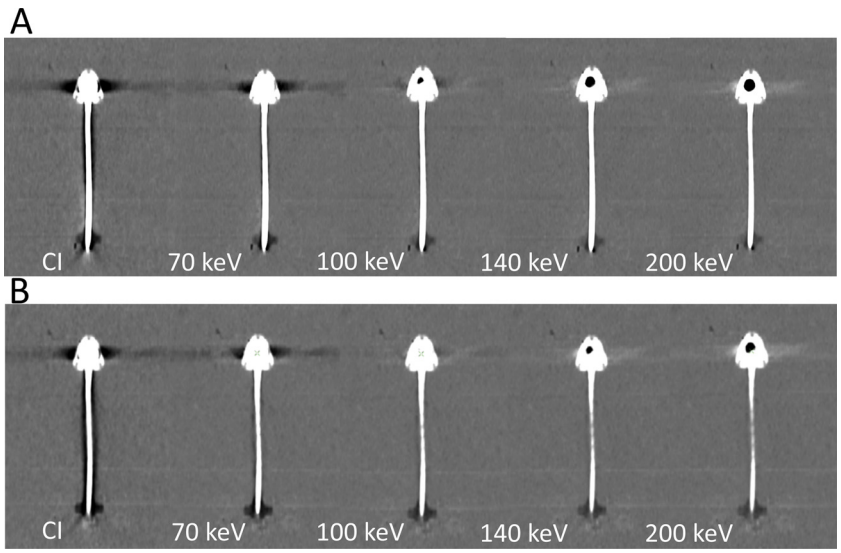

Fig. 4. Depiction of a plain port system placed in a non-anthropomorphic water phantom. Images were reconstructed as conventional (CI) and virtual monoenergetic images (VMI, 70 keV, 100 keV, 140 keV and 200 keV) in axial planes (window center/width: 60/360 for all images). (A) Depiction of a port system that was flushed after contrast media application with a saline to eliminate any contrast media residues. Hypodense and rather mild hyperdense artifacts can be seen around the port system. Artifacts are pronounced around the port chamber and the distal tip of the catheter. VMI ≥ 100 keV show an effective reduction of artifacts. Overcorrection of the initial hypodense artifacts around the port chamber can be seen in VMI ≥ 140 keV, resulting in mild hyperdense artifacts around the port chamber. (B) Depiction of a port system without saline flush after contrast media application. Compared to the flushed port system, artifacts in CI are pronounced especially around the port catheter. VMI ≥ 100 keV show an effective reduction of these artifacts; however, artifact reduction is a little less effective around the distal tip of the port catheter compared to the flushed port system.

assessment.

5. Conclusions

We found that artifacts from port systems can be effectively reduced and diagnostic assessment of surrounding soft tissue improved by virtual monoenergetic images from SDCT. Especially, if greater residues of contrast media are present within the port system and artifacts are therefore more pronounced, VMI are especially effective for artifact reduction. This might be a valuable tool in evaluating oncologic

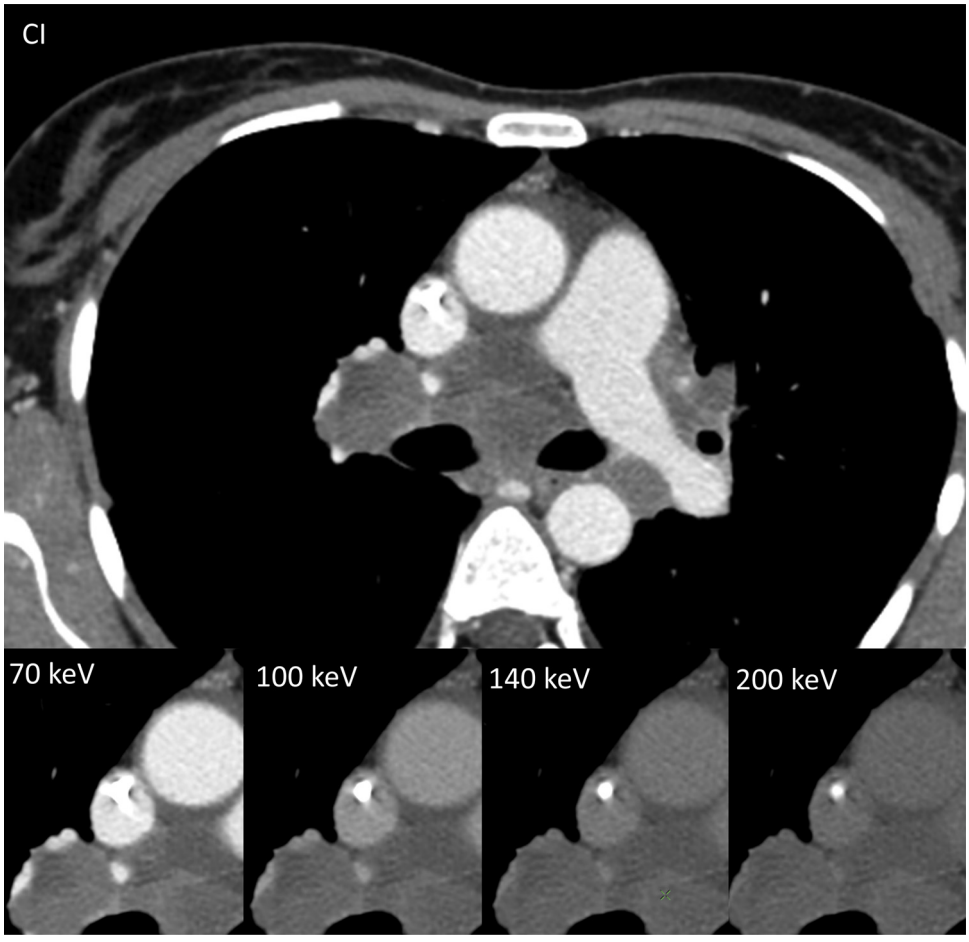

Fig. 5. Images were reconstructed as conventional (CI) and virtual monoenergetic images (VMI, 70 keV, 100 keV, 140 keV and 200 keV) in axial planes (window center/width: 60/360 for all images). Depicted is a 46-year-old patient with cervix carcinoma. The images display the distal tip of a port catheter in the superior vena cava. Hyperdense and rather mild hypodense artifacts impair the assessment of the directly bordering vessel lumen potentially impacting the detection of catheter associated thrombi. VMI ≥ 100 keV allow for an almost complete reduction of these artifacts.

Table 3
Subjective assessment of artifact reduction and surrounding tissue.

	Artifact extent				Diagnostic assessment
	Port body		Port catheter		Port body
	Hypodense	Hyperdense	Hypodense	Hyperdense	Soft tissue
CI	3 (1–4)	3 (1–4)	3 (2–4)	3 (2–3)	3 (1–5)
VMI					
70 keV	3 (1-4)	3 (1-4)	3 (2-4)	3 (2-3)	3 (1-5)
100 keV	**4 (3-5)**	**4 (3-5)**	**4 (3-5)**	**3.5 (3-4)**	**4 (3-5)**
140 keV	**4 (3-5)**	**5 (4-5)**	**4 (4-5)**	**4 (4-5)**	**5 (3-5)**
200 keV	**5 (4-5)**	**5 (4-5)**	**5 (4-5)**	**5 (3-5)**	**5 (3-5)**
ICC	0.78	0.80	0.64	0.87	0.74
p-values					
CI vs. VMI 70 keV	$p > 0.05$	$p > 0.05$	$p > 0.05$	$p > 0.05$	$p > 0.05$
CI vs. VMI 100 keV	$p < 0.001$	$p < 0.001$	$p < 0.001$	$p < 0.001$	$p < 0.001$
CI vs. VMI 140 keV	$p < 0.001$	$p < 0.001$	$p < 0.001$	$p < 0.001$	$p < 0.001$
CI vs. VMI 200 keV	$p < 0.001$	$p < 0.001$	$p < 0.001$	$p < 0.001$	$p < 0.001$

Vessels - Axillary and subclavian vessels; Soft tissue - Adjacent soft tissue (muscle, fat, lymph nodes); New artifacts - Introduction of new artifacts as compared to conventional images; ICC - Intraclass correlation; CI - Conventional images; VMI - Virtual monoenergetic images; Data is reported as median and 10/90-percent quantile.

examinations to detect soft tissue metastases and reveal port catheter associated non-occlusive thrombi.

Funding

This research did not receive any specific grant from funding agencies in the public, commercial, or not-for-profit sectors.

Disclosure

All authors approved the final article. All authors have made substantial contributions to all of the following: (1) the conception and design of the study, or acquisition of data, or analysis and interpretation of data, (2) drafting the article or revising it critically for important intellectual content, (3) final approval of the version to be submitted.

Declaration of Competing Interest

Jan Borggrefe and Nils Große Hokamp received speakers' honoraria from Philips Healthcare.

References

[1] C. Kim, D. Kim, K.Y. Lee, H. Kim, J. Cha, J.Y. Choo, P.-K. Cho, The optimal energy level of virtual monochromatic images from spectral CT for reducing beam-hardening artifacts due to contrast media in the thorax, Am. J. Roentgenol. 211 (2018) 557–563, https://doi.org/10.2214/AJR.17.19377.

[2] P. Haage, T. Schmitz-Rode, D. Hübner, W. Piroth, R.W. Günther, Reduction of contrast material dose and artifacts by a saline flush using a double power injector in helical CT of the thorax, Am. J. Roentgenol. 174 (2000) 1049–1053, https://doi.org/10.2214/ajr.174.4.1741049.

[3] D. Fleischmann, How to design injection protocols for multiple detector-row CT angiography (MDCTA), Eur. Radiol. Suppl. 15 (2005) 60–65, https://doi.org/10.1007/s10406-005-0166-x.

[4] L.M. Fayad, A. Patra, E.K. Fishman, Value of 3D CT in defining skeletal complications of orthopedic hardware in the postoperative patient, Am. J. Roentgenol. 193 (2009) 1155–1163, https://doi.org/10.2214/AJR.09.2610.

[5] M.-J. Lee, S. Kim, S.-A. Lee, H.-T. Song, Y.-M. Huh, D.-H. Kim, S.H. Han, J.-S. Suh, Overcoming artifacts from metallic orthopedic implants at high-field-Strength MR imaging and multi-detector CT, RadioGraphics 27 (2007) 791–803, https://doi.org/10.1148/rg.273065087.

[6] F.E. Boas, D. Fleischmann, CT artifacts: causes and reduction techniques, Imaging Med. 4 (2012) 229–240, https://doi.org/10.2217/iim.12.13.

[7] S. Mangold, P.M. Cannaó, U.J. Schoepf, J.L. Wichmann, C. Canstein, S.R. Fuller, G. Muscogiuri, A. Varga-Szemes, K. Nikolaou, C.N. De Cecco, Impact of an advanced image-based monoenergetic reconstruction algorithm on coronary stent visualization using third generation dual-source dual-energy CT: a phantom study, Eur. Radiol. 26 (2016) 1871–1878, https://doi.org/10.1007/s00330-015-3997-4.

[8] K.R. Laukamp, D. Zopfs, S. Lennartz, L. Pennig, D. Maintz, J. Borggrefe, N. Große Hokamp, Metal artifacts in patients with large dental implants and bridges: combination of metal artifact reduction algorithms and virtual monoenergetic images provides an approach to handle even strongest artifacts, Eur. Radiol. 29 (2019) 4228–4238, https://doi.org/10.1007/s00330-018-5928-7.

[9] D. Fleischmann, Use of high concentration contrast media: principles and rationale—vascular district, Eur. J. Radiol. 45 (2003) 88–93, https://doi.org/10.1016/S0720-048X(02)00365-0.

[10] S.S. Martin, R. Czwikla, J.L. Wichmann, M.H. Albrecht, L. Lenga, R.H. Savage, C. Arendt, R. Hammerstingl, T.J. Vogl, B. Kaltenbach, Dual-energy CT-based iodine quantification to differentiate abdominal malignant lymphoma from lymph node metastasis, Eur. J. Radiol. 105 (2018) 255–260, https://doi.org/10.1016/j.ejrad.2018.06.017.

[11] N. Takeyama, Y. Ohgiya, T. Hayashi, T. Takahashi, D. Takasu, J. Nakashima, K. Kato, Y. Kinebuchi, T. Hashimoto, T. Gokan, Comparison of different volumes of saline flush in the assessment of perivenous artefacts in the subclavian vein during cervical CT angiography, Br. J. Radiol. 84 (2011) 427–434, https://doi.org/10.1259/bjr/86966343.

[12] N. Große Hokamp, V. Neuhaus, N. Abdullayev, K. Laukamp, S. Lennartz, A. Mpotsaris, J. Borggrefe, Reduction of artifacts caused by orthopedic hardware in the spine in spectral detector CT examinations using virtual monoenergetic image reconstructions and metal-artifact-reduction algorithms, Skeletal Radiol. 47 (2017) 195–201, https://doi.org/10.1007/s00256-017-2776-5.

[13] C.H. McCollough, S. Leng, L. Yu, J.G. Fletcher, Dual- and multi-energy CT: principles, technical approaches, and clinical applications, Radiology 276 (2015) 637–653, https://doi.org/10.1148/radiol.2015142631.

[14] R.E. Alvarez, A. Macovski, Energy-selective reconstructions in X-ray computerized tomography, Phys. Med. Biol. 21 (1976) 733–744, https://doi.org/10.1088/0031-9155/21/5/002.

[15] M.H. Albrecht, J. Trommer, J.L. Wichmann, J.-E. Scholtz, S.S. Martin, T. Lehnert, T.J. Vogl, B. Bodelle, Comprehensive comparison of virtual monoenergetic and linearly blended reconstruction techniques in third-generation dual-source dual-energy computed tomography angiography of the thorax and abdomen, Invest. Radiol. 51 (2016) 582–590, https://doi.org/10.1097/RLI.0000000000000272.

[16] A.P. Sauter, D. Muenzel, J. Dangelmaier, R. Braren, F. Pfeiffer, E.J. Rummeny, P.B. Noël, A.A. Fingerle, Dual-layer spectral computed tomography: virtual non-contrast in comparison to true non-contrast images, Eur. J. Radiol. 104 (2018) 108–114, https://doi.org/10.1016/j.ejrad.2018.05.007.

[17] N. Große Hokamp, K.R. Laukamp, S. Lennartz, D. Zopfs, N. Abdullayev, V.F. Neuhaus, D. Maintz, J. Borggrefe, Artifact reduction from dental implants using virtual monoenergetic reconstructions from novel spectral detector CT, Eur. J. Radiol. 104 (2018) 136–142, https://doi.org/10.1016/j.ejrad.2018.04.018.

[18] K.R. Laukamp, S. Lennartz, V.-F. Neuhaus, N. Große Hokamp, R. Rau, M. Le Blanc, N. Abudullayev, A. Mpotaris, D. Maintz, J. Borggrefe, CT metal artifacts in patients with total hip replacements: for artifact reduction monoenergetic reconstructions and post-processing algorithms are both efficient but not similar, Eur. Radiol. 28 (2018) 4524–4533, https://doi.org/10.1007/s00330-018-5414-2.

[19] Y. Jia, J. Zhang, J. Fan, C. Li, Y. Sun, D. Li, X. Xiao, Gemstone spectral imaging reduced artefacts from metal coils or clips after treatment of cerebral aneurysms: a retrospective study of 35 patients, Br. J. Radiol. 88 (2015) 20150222, , https://doi.org/10.1259/bjr.20150222.

[20] S. Winklhofer, R. Hinzpeter, D. Stocker, G. Baltsavias, L. Michels, J.-K. Burkhardt, L. Regli, A. Valavanis, H. Alkadhi, Combining monoenergetic extrapolations from dual-energy CT with iterative reconstructions: reduction of coil and clip artifacts from intracranial aneurysm therapy, Neuroradiology 60 (2018) 281–291, https://doi.org/10.1007/s00234-018-1981-9.

[21] S.H. Lee, S.J. Yun, D.H. Kim, H.H. Jo, J.G. Song, Y.S. Park, Diagnostic usefulness of low-dose lumbar multi-detector CT with iterative reconstruction in trauma patients: acomparison with standard-dose CT, Br. J. Radiol. 90 (2017) 20170181, , https://doi.org/10.1259/bjr.20170181.

[22] I. Khodarahmi, R.R. Haroun, M. Lee, G.S.K. Fung, M.K. Fuld, L.C. Schon, E.K. Fishman, J. Fritz, Metal artifact reduction computed tomography of arthroplasty implants, Invest. Radiol. 53 (2018) 728–735, https://doi.org/10.1097/RLI.0000000000000497.

[23] J. James, M. Teo, V. Ramachandran, M. Law, D. Stoney, M. Cheng, A critical review of the chest CT scans performed to detect asymptomatic synchronous metastasis in new and recurrent breast cancers, World J. Surg. Oncol. 17 (2019) 40, https://doi.org/10.1186/s12957-019-1584-x.

[24] G. Rauthe, C. Altmann, Complications in connection with venous port systems: prevention and therapy, Eur. J. Surg. Oncol. 24 (1998) 192–198, https://doi.org/10.1016/S0748-7983(98)92963-8.

[25] L.I. Ma, Y. Liu, J. Wang, Y. Chang, L. Yu, C. Geng, Totally implantable venous access port systems and associated complications: a single-institution retrospective analysis of 2,996 breast cancer patients, Mol. Clin. Oncol. 4 (2016) 456–460, https://doi.org/10.3892/mco.2016.726.

[26] M.H. Albrecht, J.-E. Scholtz, K. Hüsers, M. Beeres, A.M. Bucher, M. Kaup, S.S. Martin, S. Fischer, B. Bodelle, R.W. Bauer, T. Lehnert, T.J. Vogl, J.L. Wichmann, Advanced image-based virtual monoenergetic dual-energy CT angiography of the abdomen: optimization of kiloelectron volt settings to improve image contrast, Eur. Radiol. 26 (2016) 1863–1870, https://doi.org/10.1007/s00330-015-3970-2.

[27] C.N. De Cecco, D. Caruso, U.J. Schoepf, D. De Santis, G. Muscogiuri, M.H. Albrecht, F.G. Meinel, J.L. Wichmann, P.F. Burchett, A. Varga-Szemes, D.H. Sheafor, A.D. Hardie, A noise-optimized virtual monoenergetic reconstruction algorithm improves the diagnostic accuracy of late hepatic arterial phase dual-energy CT for the detection of hypervascular liver lesions, Eur. Radiol. 28 (2018) 3393–3404, https://doi.org/10.1007/s00330-018-5313-6.

[28] S.J. Riederer, C.A. Mistretta, Selective iodine imaging using *K* -edge energies in computerized x-ray tomography, Med. Phys. 4 (1977) 474–481, https://doi.org/10.1118/1.594357.

[29] M.H. Albrecht, M.W. Bickford, U.J. Schoepf, C. Tesche, D. De Santis, M. Eid, B.E. Jacobs, T.M. Duguay, B.T. Schmidt, C. Canstein, A. Varga-Szemes, D. Leithner, S. Martin, T.J. Vogl, C.N. De Cecco, Beam-hardening in 70-kV Coronary CT angiography: artifact reduction using an advanced post-processing algorithm, Eur. J. Radiol. 101 (2018) 111–117, https://doi.org/10.1016/j.ejrad.2018.02.016.

[30] M.N. Bongers, C. Schabel, C. Thomas, R. Raupach, M. Notohamiprodjo, K. Nikolaou, F. Bamberg, Comparison and combination of dual-energy- and iterative-based metal artefact reduction on hip prosthesis and dental implants, PLoS One 10 (2015) e0143584, , https://doi.org/10.1371/journal.pone.0143584.